Sensitivity of Antarctic sea level contribution to bed friction inversion choices in the BISICLES ice sheet model

Jonathan R Barnsley[1], Tamsin L Edwards[1], Alex Bradley[1], Stephen L Cornford[2], and Matt Trevers[2]

[1]King's College London, Department of Geography, London, UK
[2]University of Bristol, Department of Geography, Bristol, UK

Correspondence: Jonathan R Barnsley (jonathan.barnsley@kcl.ac.uk)

Abstract. Antarctica is the largest potential contributor to future sea level but is also the most uncertain. The ice sheet initial state is known to be a significant source of uncertainty, but this uncertainty is rarely explored outside of large-scale model intercomparison projects.

Century-scale projections of the Antarctic ice sheet typically generate an initial state by solving an inverse problem for basal friction — and sometimes other fields — such that modelled ice velocities closely match observations. While this yields realistic short-term behaviour, it may also overfit by masking deficiencies elsewhere in the model.

Few modelling studies explicitly treat the inverse problem itself as a source of uncertainty. There is some evidence that regularisation choices within the inversion can produce uncertainty comparable to other commonly perturbed ice sheet model parameters, though this is limited to select experimental setups. It is unknown whether these results translate to other ice sheet models or domains.

Here, we use the BISICLES ice sheet model to explore inverse problems as a source of uncertainty in Antarctica's future sea level contribution. We generate an ensemble of initial states and project them forward to 2300 under a high-emission scenario. We assess the sensitivity of sea level projections to regularisation parameters within the inversion and compare it against other commonly perturbed parameters. We find that the sensitivity to regularisation in BISICLES is generally lower than other parameters and that this gap widens on longer timescales.

1 Introduction

2 Methods

2.1 BISICLES ice sheet model

BISICLES (Cornford et al., 2013) is an adaptive mesh, vertically integrated ice sheet model, which has been used extensively for century-scale modelling of the Antarctic ice sheet (Cornford et al., 2015; Siahaan et al., 2022; O'Neill et al., 2025). It uses the L1L2 approximation to Stokes flow (Schoof and Hindmarsh, 2010), which incorporates both membrane stresses and a simplified treatment of vertical shear. This allows BISICLES to simulate a wide range of flow regimes in Antarctica with computational efficiency. Here, we run BISICLES with a base resolution of 8 km and 3 layers of refinement, up to 1 km at the

grounding line and in regions of fast-flowing ice. This resolution significantly improves the represenation of grounding line dynamics compared to coarser grids (Cornford et al., 2016).

BISICLES solves the 2-dimensional L1L2 mass transport and stress balance equations outlined in Cornford et al. (2015). They feature a vertically integrated effective viscosity, $\phi h\bar{\mu}$, defined by:

$$\phi h\bar{\mu}(x,y) = \phi \int_{s-h}^{s} \mu(x,y,z)dz, \tag{1}$$

where h is ice thickness, s is surface elevation, and ϕ is an uncertain, spatially-varying coefficient that we estimate using inverse methods. ϕ can be interpreted as a damage multiplier and typically takes values between 0.05 and 1, with lower values in regions close to the grounding line or in fast-flowing ice streams. The vertically varying effective viscosity, $\mu(x,y,z)$, is calculated using the Glen-Steinemann flow law (Glen, 1955):

$$\mu(x,y,z) = \frac{1}{2A_0 A(T)\tau^{n-1}}, \tag{2}$$

where $A(T)$ is a temperature-dependant Paterson rate factor (Cuffey and Paterson, 2010). The 3-dimensional temperature field is derived from a 100,000-year thermal spin-up described in Trevers et al. (2024). τ is the deviatoric stress tensor and the flow law exponent n is an uncertain parameter that we perturb in the ensemble. A correction factor, $A_0 = 100,000^{(3-n)}$, ensures that the effective viscosity is independant of n at a reference stress of 100 kPa. Either side of this value, the flow law diverges from the $n = 3$ case, but the effective viscosity is scaled by ϕ during the inverse problem so that the initial state matches observed ice velocities.

Basal sliding is governed by a pressure-limited Weertman-Coulomb sliding law derived from Tsai et al. (2015), which allows for Weertman and Coulomb-like behaviour over hard and soft beds, respectively. The basal shear stress, τ_b, is given by:

$$\tau_b = -\min(\tau_w, \tau_c)\frac{\mathbf{u}}{|\mathbf{u}|}, \tag{3}$$

where τ_w has a power-law relationship with the velocity $\mathbf{u}$, and τ_c is a Coulomb-limiting term defined by the effective pressure, N:

$$\tau_w = C|\mathbf{u}|^m, \tag{4}$$

$$\tau_c = \frac{1}{2}N. \tag{5}$$

C is a spatially varying friction coefficient that, along with the viscosity coefficient, ϕ, is determined via an inverse problem. We treat the friction exponent m as an uncertain parameter which is to be perturbed in the ensemble. This sliding law has been used in previous BISICLES experiments (O'Neill et al., 2025) and performs similarly to other common sliding laws in Antarctica (Barnes and Gudmundsson, 2022).

2.2 Model initialisation

We initialise BISICLES using an inverse method to solve for the basal friction coefficient, C, and the viscosity coefficient, ϕ, such that modelled surface velocities closely match observations. BISICLES uses conjugate gradient descent (Shewchuk,

1994) to minimise a cost function, J, defined by:

$$J = J_m + J_p, \tag{6}$$

where J_m is a function of the velocity misfit

$$J_m = \frac{1}{2} \int_{\Omega_V} (|\mathbf{u}| - |\mathbf{u}_{obs}|)^2 d\Omega_V, \tag{7}$$

and J_p is a Tikhonov penalty function

$$J_p = \frac{\alpha_C}{2} \int_{\Omega_V} |\nabla C|^2 d\Omega_V + \frac{\alpha_\phi}{2} \int_{\Omega_V} |\nabla \phi|^2 d\Omega_V. \tag{8}$$

α_C and α_ϕ are regularisation parameters that control the smoothness of C and ϕ, respectively, and are both perturbed in our ensemble. Ω_V is the domain over which velocities are observed, and $\mathbf{u}_{obs}$ are the observed surface velocities from Rignot et al. (2017).

Since the Tsai sliding law is independent of C in areas of low hydrostatic pressure, we solve the inverse problem using a simple linear sliding law that constrains C everywhere. For ensemble members with $m \neq 1$, we then adjust C post-inversion such that basal drag (and therefore ice velocity) is equal on either side of the initialisation. This is done by scaling C according to

$$C_m = C_{(m=1)} \left(|\mathbf{u}| + \epsilon\right)^{1-m}, \tag{9}$$

where $\epsilon = 10^{-5}$ is a small regularising term to prevent infinite friction values. Ideally, this would yield the same solution for basal friction regardless of the value of m used in the inversion, although there can be differences due to the path-dependence of the solution (Wolovick et al., 2023). Nonetheless, we found that inversions with a linear sliding law were faster and more convenient that with $m \neq 1$.

The initial ice geometry is taken from BedMachine Antarctica v2 (Morlighem, 2020), the initial guess for ϕ is uniformly 1, and the initial guess for C is calculated by equating basal drag to the driving stress. This yields

$$C_{init} = \rho g h \nabla s |\mathbf{u}|^{-1}, \tag{10}$$

where $\rho = 917 kgm^{-3}$ is the density of ice and $g = 9.81$ is gravitational acceleration.

A common issue with inverse methods is that the period immediately following initialisation can feature a short-term shock as the ice sheet adjusts to inconsistencies between the geometry and modelled physics. Inversions are then typically followed by a short relaxation period to allow the ice sheet to settle before projections begin. This, however, allows surface ice velocities to drift from their observed values used during the inversion. Modern BISICLES experiments try to resolve this by alternating inverse problems with short periods of relaxation, during which the ice geometry is allowed to evolve (Bevan et al., 2023; Trevers et al., 2024). We follow a similar approach here, solving an inverse problem every year of a 15-year relaxation. During the relaxation, the thickness of floating ice shelves is held constant and we apply a surface mass balance from the MAR regional climate model (Agosta et al., 2019).

2.3 Climate forcing

Inverse methods produce a good fit to observed velocities, but this often results in poor fits to other measurables such as the rate of elevation change, $\dot{h}$. We could incorporate additional terms into the cost function (7) to mitigate this, but these would come at a cost to the velocity misfit. Model outputs can also be very sensitive to the balance between the velocity and $\dot{h}$ components of a misfit function (Rosier et al., 2025). Instead, we choose to correct for bias in $\dot{h}$ by exploiting uncertainty in the surface mass balance. We apply a background rate of surface mass balance that is designed to bridge the gap between modelled and observed $\dot{h}$:

$$\mathrm{SMB}_{bkg} = \dot{h}_{obs} + \nabla \cdot (\mathbf{u}h) \tag{11}$$

where $\dot{h}_{obs}$ is the observed rate of elevation change from (Smith et al., 2020) and $\nabla \cdot (\mathbf{u}h)$ is the flux divergence at the end of a relaxation with default parameter values. We set bounds of -1–2 ma^{-1} and apply a Gaussian filter to smooth out short-wavelength components of the flux divergence (Nias et al., 2016). The main effect of this is to correct a thickening bias over the Antarctic Peninsula and trans-Antarctic mountains, where our 1 km grid resolution is too coarse to resolve the dynamics of these smaller glaciers.

On top of this background SMB, we apply a time-varying anomaly from the CESM2-WACCM climate model

2.4 Experimental design

3 Results

We project our initial states forward with the CESM2 climate forcing up to 2300 and calculate total Antarctic sea level contribution for each ensemble member (Figure 1). The ensemble range at 2100 is ??–?? m, which compares well with the IPCC AR6 range of 0.03–0.28 m under SSP5–8.5 (cite IPCC). In the 22nd and 23rd centiries, all ensemble members accelerate their mass loss and the range widens to ??–?? m by 2300.

The spatial patterns of ice thickness change are broadly similar across the ensemble, with most mass loss occuring in regions of West Antarctica: the Amundsen Sea sector, the Siple coast, and the Weddell sea sector. However, the extent of mass loss in these regions depends on parameter choices, with high variance along Thwaites, Foundations, and Denman glaciers (Figure 2). Some areas of low variance also show regions that retreat in all ensemble members, including the collapse of Pine Island Glacier and the Ross and Filchner-Ronne ice shelves.

For each parameter, we calculate the range in sea level contribution between ensemble members with minimal and maximal values of that parameter. This provides a rudimentary measure of sensitivity, which we can compare across parameters. Figure 3 highlights the timescale-dependance of this sensitivity, with different relative importance of parameters at 2100 and 2300.

At 2100, the largest sensitivity is to ice shelf basal melt, γ, but this reduces in relative terms by 2300 as other parameters become more important. Sensitivity to the flow law exponent, n, and the basal sliding exponent, m, both increase over time and are comparable to γ by 2300. Sensitivities to glacial isostatic adjustment (UMV) and bed friction regularisation (a_C) are

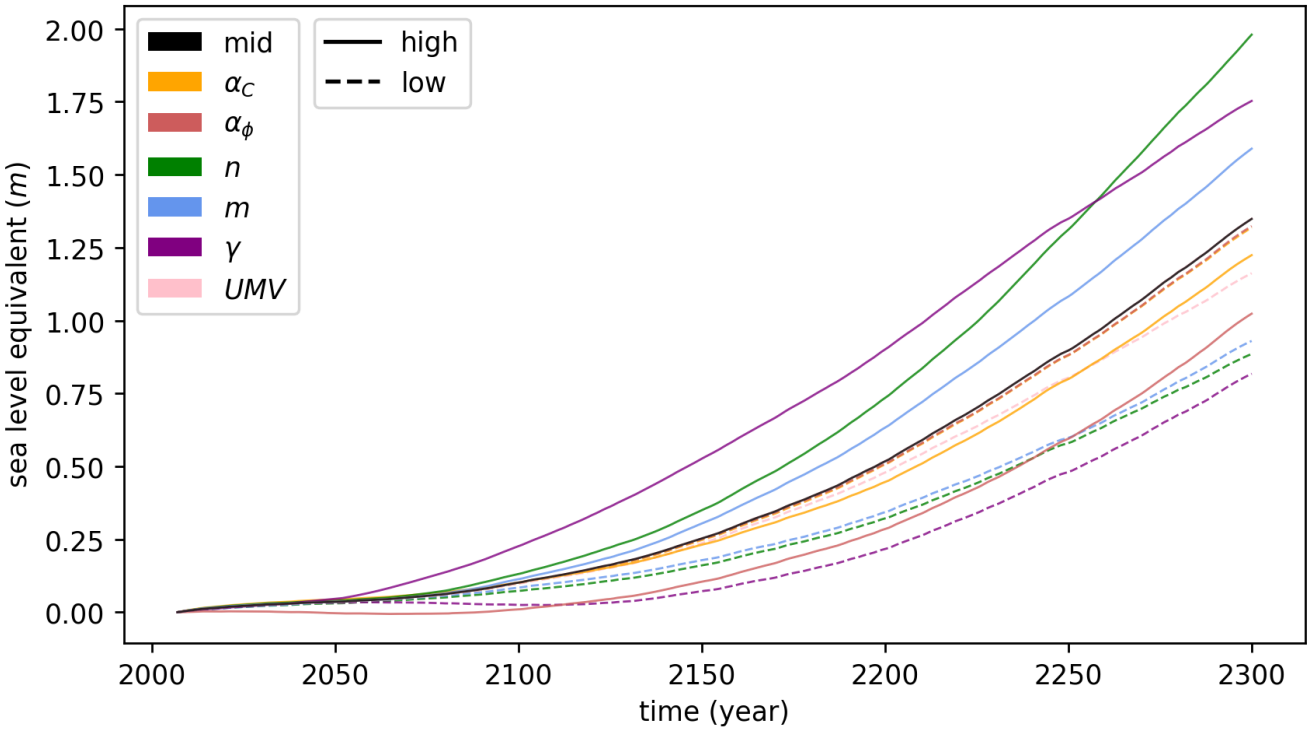

Figure 1. Timeseries of Antarctic sea level contribution for high and low values of each perturbed parameter.

negligible at 2100 and remain small by 2300. Sensitivity to regularisation of the viscosity coefficient, a_ϕ, is the second largest of all parameters by 2100 but becomes less significant relative to other parameters by 2300.

4 Discussion

The most direct comparison for our results is with (cite Rosier), who simulate the Amundsen Sea Embayment (ASE) up to 2100 using the Ùa ice sheet model. Inversions in Ùa are similar to those in BISICLES, using the adjoint method to solve for basal friction and the rate factor, which is analogous to the viscosity coefficient in BISICLES insofar as it controls ice rheology. Similar to Rosier et al., we find that regularisation parameters in the initialisation can be a significant source of uncertainty in century-scale sea level projections. However, there are some notable differences between our results.

Both studies agree that sensitivity to 'rheology-related' regularisation (rate factor in Ùa, viscosity coefficient in BISICLES) is higher than sensitivity to bed friction regularisation. In BISICLES, the viscosity coefficient plays a critical role in dynamics near to the present-day grounding line, which are highly influential in short-term sea level projections. However, we find that this sensitivity decreases on longer timescales, possibly because the ice sheet retreats past present-day grounding lines into regions where the viscosity coefficient is mostly uniform.

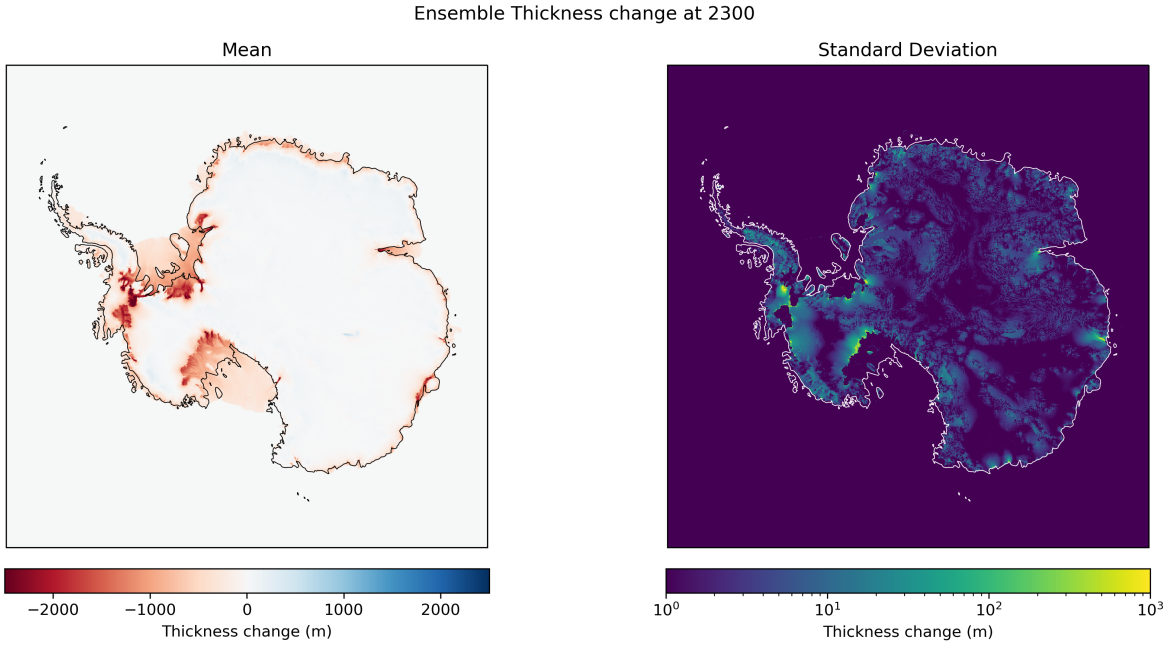

Figure 2. Timeseries of Antarctic sea level contribution for high and low values of each perturbed parameter.

Basal friction plays a role throughout the ice sheet and particularly in the ice streams, which may explain why sensitivity to its regularisation increases relative to rheology-related regularisation on longer timescales. However, sensitivity to bed friction regularisation in BISICLES is much lower than in Ùa when compared against other commonly perturbed parameters. This may be due to differences in the domain and resolution of the models. The inclusion of slow-moving parts of East Antarctica in our simulations introduces very high friction values that may dominate the Tikhonov penalty function, focusing the smoothing on areas of Antarctica that are less dynamically important to century-scale sea level projections. BISICLES is also known to be sensitive to grid resolution up to at least 500 m (cite steph 2016), and our 1 km resolution may be too coarse to fully capture the influence of bed friction regularisation on ice dynamics.

The timescale dependance of our results highlight the importance of considering the projection period and forcing when assessing sources of uncertainty. Because of the very high CESM2-WACCM forcing post-2100, the major ice shelves collapse in all ensemble members before 2300, which reduces sensitivity to ice shelf basal melt relative to other parameters on this timescale. Similarly, the collapse of Pine Island Glacier in all ensemble members affects the sensitivity of our outputs to key parameters in that region, which could include bed friction regularisation. If we had used a less extreme forcing — either a lower-emission scenario or a different climate model — we may have found different patterns of sensitivity. Rosier et al find that parameters generally have higher sensitivity in a high-emissions scenario compared to a low-emissions scenario, but that this pattern is often reversed for initialisation parameters, supporting this idea.

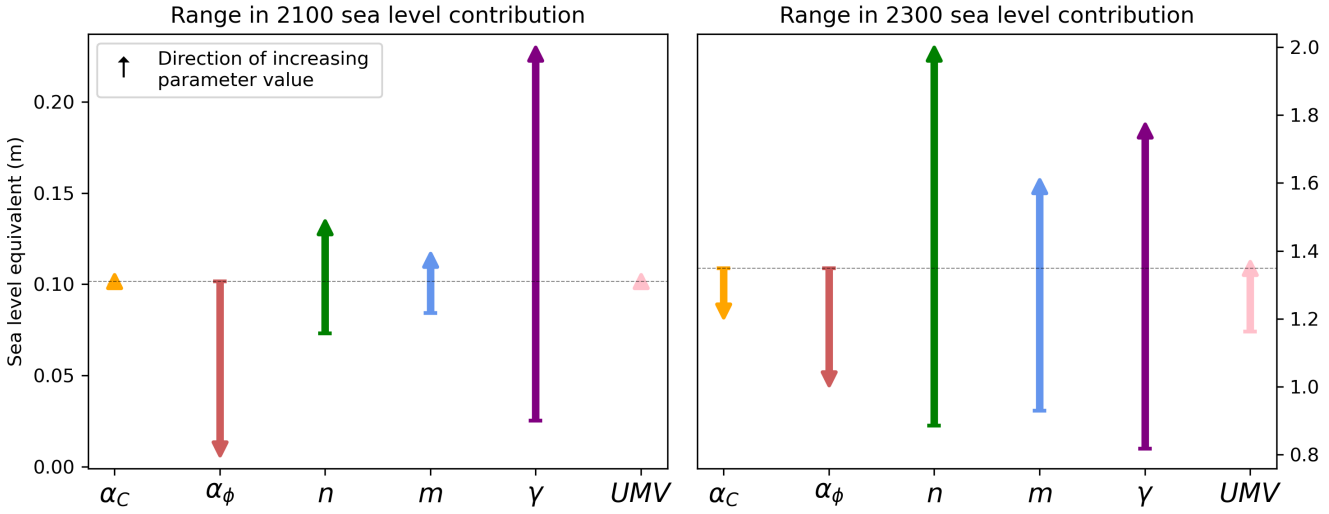

Figure 3. Sensitivity of Antarctic sea level contribution to each perturbed parameter at (a) 2100 and (b) 2300. Arrows denote the range in sea level contribution between ensemble members with minimal and maximal values of that parameter, pointing from minimal to maximal. Arrows pointing upwards/downwards therefore indicate a parameter that increases/decreases sea level contribution with higher values. The dashed horizontal line indicates the sea level contribution in a simulation with all parameters held at their default value.

5 Conclusions

• The sensitivity of Antarctic SLC to regularisation parameters may be dependent on the model, forcing, timescale, domain, and resolution used in the experiment. • Results are likely to also vary with the type of regularisation and gradient descent used in the inverse problem (sort of included in 'model'). • 'Initial state uncertainty' as seen in initMIP is still much larger than what we have explored here, which makes sense because it covers multiple initialisation techniques. • Using range as a measure of sensitivity is less preferable to something such as Sobol' sensitivity. However, these quick tests provide a basis to then go on and do larger PPEs.

Code availability. TEXT

Data availability. TEXT

Code and data availability. TEXT

Sample availability. TEXT

Video supplement. TEXT

Appendix A

A1

Author contributions. TEXT

Competing interests. TEXT

Disclaimer. TEXT

Acknowledgements. TEXT

References

Agosta, C., Amory, C., Kittel, C., Orsi, A., Favier, V., Gallée, H., Van Den Broeke, M. R., Lenaerts, J. T. M., Van Wessem, J. M., Van De Berg, W. J., and Fettweis, X.: Estimation of the Antarctic Surface Mass Balance Using the Regional Climate Model MAR (1979–2015) and Identification of Dominant Processes, The Cryosphere, 13, 281–296, https://doi.org/10.5194/tc-13-281-2019, 2019.

Barnes, J. M. and Gudmundsson, G. H.: The Predictive Power of Ice Sheet Models and the Regional Sensitivity of Ice Loss to Basal Sliding Parameterisations: A Case Study of Pine Island and Thwaites Glaciers, West Antarctica, The Cryosphere, 16, 4291–4304, https://doi.org/10.5194/tc-16-4291-2022, 2022.

Bevan, S., Cornford, S., Gilbert, L., Otosaka, I., Martin, D., and Surawy-Stepney, T.: Amundsen Sea Embayment Ice-Sheet Mass-Loss Predictions to 2050 Calibrated Using Observations of Velocity and Elevation Change, Journal of Glaciology, 69, 1729–1739, https://doi.org/10.1017/jog.2023.57, 2023.

Cornford, S. L., Martin, D. F., Graves, D. T., Ranken, D. F., Le Brocq, A. M., Gladstone, R. M., Payne, A. J., Ng, E. G., and Lipscomb, W. H.: Adaptive Mesh, Finite Volume Modeling of Marine Ice Sheets, Journal of Computational Physics, 232, 529–549, https://doi.org/10.1016/j.jcp.2012.08.037, 2013.

Cornford, S. L., Martin, D. F., Payne, A. J., Ng, E. G., Le Brocq, A. M., Gladstone, R. M., Edwards, T. L., Shannon, S. R., Agosta, C., van den Broeke, M. R., Hellmer, H. H., Krinner, G., Ligtenberg, S. R. M., Timmermann, R., and Vaughan, D. G.: Century-Scale Simulations of the Response of the West Antarctic Ice Sheet to a Warming Climate, The Cryosphere, 9, 1579–1600, https://doi.org/10.5194/tc-9-1579-2015, 2015.

Cornford, S. L., Martin, D. F., Lee, V., Payne, A. J., and Ng, E. G.: Adaptive Mesh Refinement versus Subgrid Friction Interpolation in Simulations of Antarctic Ice Dynamics, Annals of Glaciology, 57, 1–9, https://doi.org/10.1017/aog.2016.13, 2016.

Cuffey, K. M. and Paterson, W. S. B.: The Physics of Glaciers, Elsevier, San Diego, fourth edition edn., ISBN 978-0-12-369461-4 978-0-08-091912-6, 2010.

Glen, J. W.: The Creep of Polycrystalline Ice, Proceedings of the Royal Society of London. Series A. Mathematical and Physical Sciences, 228, 519–538, https://doi.org/10.1098/rspa.1955.0066, 1955.

Morlighem, M.: MEaSUREs BedMachine Antarctica, Version 2, https://doi.org/10.5067/E1QL9HFQ7A8M, 2020.

Nias, I. J., Cornford, S. L., and Payne, A. J.: Contrasting the Modelled Sensitivity of the Amundsen Sea Embayment Ice Streams, Journal of Glaciology, 62, 552–562, https://doi.org/10.1017/jog.2016.40, 2016.

O'Neill, J. F., Edwards, T. L., Martin, D. F., Shafer, C., Cornford, S. L., Seroussi, H. L., Nowicki, S., Adhikari, M., and Gregoire, L. J.: ISMIP6-based Antarctic Projections to 2100: Simulations with the BISICLES Ice Sheet Model, The Cryosphere, 19, 541–563, https://doi.org/10.5194/tc-19-541-2025, 2025.

Rignot, E., Mouginot, J., and Scheuchl, B.: MEaSUREs InSAR-Based Antarctica Ice Velocity Map, Version 2, https://doi.org/10.5067/D7GK8F5J8M8R, 2017.

Rosier, S. H. R., Gudmundsson, G. H., Jenkins, A., and Naughten, K. A.: Calibrated Sea Level Contribution from the Amundsen Sea Sector, West Antarctica, under RCP8.5 and Paris 2C Scenarios, The Cryosphere, 19, 2527–2557, https://doi.org/10.5194/tc-19-2527-2025, 2025.

Schoof, C. and Hindmarsh, R. C. A.: Thin-Film Flows with Wall Slip: An Asymptotic Analysis of Higher Order Glacier Flow Models, The Quarterly Journal of Mechanics and Applied Mathematics, 63, 73–114, https://doi.org/10.1093/qjmam/hbp025, 2010.

Shewchuk, J. R.: An Introduction to the Conjugate Gradient Method without the Agonizing Pain, Tech. rep., Carnegie Mellon University, USA, 1994.

Siahaan, A., Smith, R. S., Holland, P. R., Jenkins, A., Gregory, J. M., Lee, V., Mathiot, P., Payne, A. J., Ridley, J. K., and Jones, C. G.: The Antarctic Contribution to 21st-Century Sea-Level Rise Predicted by the UK Earth System Model with an Interactive Ice Sheet, The Cryosphere, 16, 4053–4086, https://doi.org/10.5194/tc-16-4053-2022, 2022.

Smith, B., Fricker, H. A., Gardner, A. S., Medley, B., Nilsson, J., Paolo, F. S., Holschuh, N., Adusumilli, S., Brunt, K., Csatho, B., Harbeck, K., Markus, T., Neumann, T., Siegfried, M. R., and Zwally, H. J.: Pervasive Ice Sheet Mass Loss Reflects Competing Ocean and Atmosphere Processes, Science, 368, 1239–1242, https://doi.org/10.1126/science.aaz5845, 2020.

Trevers, M., Cornford, S. L., Payne, A. J., Gasson, E., and Bevan, S. L.: Retreat of Thwaites Glacier Triggered by Its Neighbours, https://doi.org/10.22541/essoar.170957499.97583808/v1, 2024.

Tsai, V. C., Stewart, A. L., and Thompson, A. F.: Marine Ice-Sheet Profiles and Stability under Coulomb Basal Conditions, Journal of Glaciology, 61, 205–215, https://doi.org/10.3189/2015JoG14J221, 2015.

Wolovick, M., Humbert, A., Kleiner, T., and Rückamp, M.: Regularization and L-curves in Ice Sheet Inverse Models: A Case Study in the Filchner–Ronne Catchment, The Cryosphere, 17, 5027–5060, https://doi.org/10.5194/tc-17-5027-2023, 2023.